Distribution and Structure of N Atoms in Multiwalled Carbon Nanotubes Using Variable-Energy X-Ray Photoelectron Spectroscopy

Hyun Chul Choi and Jeunghee Park*

Department of Chemistry, Korea University, Jochiwon 339-700, Korea

Bongsoo Kim*

Department of Chemistry, KAIST, Daejeon 305-701, Korea

Received: October 14, 2004; In Final Form: December 21, 2004

We investigated the inhomogeneous distribution of concentration and electronic structure of the nitrogen (N) atoms doped in the multiwalled carbon nanotubes (CNTs) by variable-energy X-ray photoelectron spectroscopy (XPS), X-ray absorption near-edge structure, and electron energy-loss spectroscopy. The vertically aligned N-doped CNTs on the substrates were grown via pyrolysis of iron phthalocyanine (FePc), cobalt phthalocyanine (CoPc), and nickel phthalocyanine (NiPc) in the temperature range 750−1000 °C. They usually have a bamboo-like structure, and the diameter is in the range of 15−80 nm. As the photon energy of XPS increases from 475 to 1265 eV, the N content increases up to 8 atomic %, indicating a higher N concentration at the inside of nanotubes. We identified three typed N structures: graphite-like, pyridine-like, and molecular N_2. The pyridine-like N structure becomes significant at the inner walls. Molecular N_2 would exist as intercalated forms in the vicinity of hollow inside. The XPS valence band analysis reveals that the pyridine-like N structure induces the metallic behaviors. The CNTs grown using NiPc contain the higher content of pyridine-like structure compared to those grown using FePc and CoPc, so they exhibit more metallic properties.

1. Introduction

Carbon nanotubes (CNTs) are currently attractive materials for a diverse range of applications because of their extraordinary mechanical and electrical properties.[1,2] The important potential application includes field emission displays (FED)[3,4] and nanoscale electronic devices.[5−8] Many of these applications are based on the electrical properties of CNTs, which strongly depend on their helicity and diameter.[9] Therefore, the control of electrical properties is very important in many applications of CNTs. The doping of CNTs with other chemical elements (e.g., B or N) is a practical and feasible way to tailor their electrical properties. The N-doped CNTs show indeed n-type behavior regardless of a tube chirality.[10]

The diverse electronic structures of CN_x films have been proposed, including diamond-like C_3N_4, graphite-like (N atoms replacing C atoms in graphite layers), pyridine-like, pyrrolic, and triple-bonded CN.[11−14] Much attention has directed to find the similarity or difference between the electronic structure of the N-doped CNTs and the CN_x film. Dos Santos and Alvarez predict a possibility of graphite-like structured single-walled nanotubes with elemental composition C:N = 1:1 using semiempirical pseudopotential methods.[15] The possibility of superhard C_3N_4 single-walled nanotubes was also proposed by Miyamoto et al.[16] Terrones group showed that the pyridine-like N structures are responsible for the metallic properties of the N-doped CNTs using scanning tunneling spectrum and tight binding/ab initio calculations.[10] Terrones and Walton groups proposed that gaseous N_2 can be encapsulated within the hollow nanotube core and released by electron irradiation, using electron energy-loss spectroscopy (EELS).[17,18] The graphite-like, pyridine-like, pyrrolic, and cross-linked sp^3 structures in the N-doped CNTs were identified by X-ray photolelectron spectroscopy (XPS).[19−23]

Another important issue is the distribution of those diverse N structures inside the CNT. The EELS across the N-doped CNTs shows that the N atoms exist mainly as gaseous N_2 encapsulated in the hollow nanotube core.[17,18,24] It was also reported that the N concentration of the inner parts or compartment layers is higher than that of the wall.[25−27] These findings indicate that the electronic structure of doped N atoms can be inhomogeneous inside the CNTs. But there are few studies for the radially resolved distribution of the electronic structure of doped N atoms in CNTs.

Considering the ongoing scientific and technological efforts, therefore, there is a need for better understanding of the electronic structure of doped N atoms as well as their distribution. Here, we employed variable-energy XPS, X-ray absorption near-edge structure (XANES), and EELS, to obtain the information of the electronic structure of doped N atoms in mutiwalled carbon nanotubes (MWNTs). Since the escape depth of a photoelectron increases with its kinetic energy, the higher photon energy provides more information for the inner parts of CNTs.[28] In the present work the photon energy of XPS varies in the range 360−1265 eV. The vertically aligned N-doped CNTs were synthesized with high purity on the silicon oxide substrates via pyrolysis of iron phthalocyanine ($FeC_{32}N_8H_{16}$, designated as FePc hereafter), cobalt phthalocyanine (CoPc), and nickel phthalocyanine (NiPc) in the temperature range 750−1000 °C.

2. Experimental Section

The vertically aligned CNTs were grown via pyrolysis of FePc, CoPc, and NiPc, using the method as described in ref 29. The CNTs were grown from FePc at 750, 800, 900, and

* Corresponding authors. E-mails: parkjh@korea.ac.kr; bongsoo@kaist.ac.kr.

10.1021/jp0453109 CCC: $30.25
Published on Web 02/19/2005

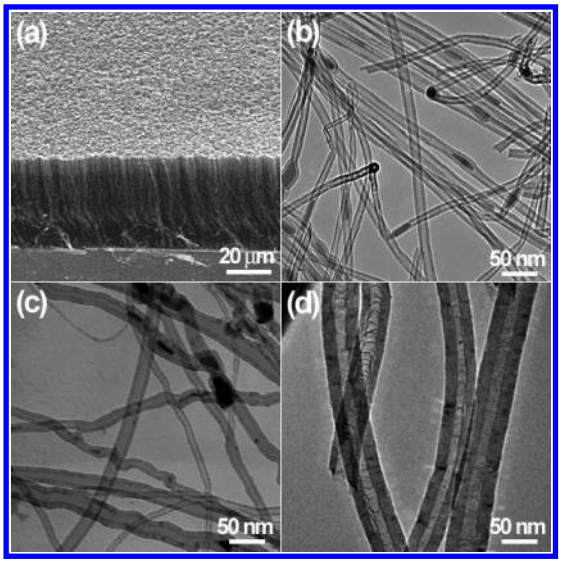

Figure 1. (a) SEM micrographs of the vertically aligned CNTs grown on the substrates (Fe-900). TEM images of (b) Fe-900, (c) Co-900, and (d) Ni-900.

1000 °C. We denote the sample as Fe-750, Fe-800, Fe-900, and Fe-1000, respectively. The CNTs were also grown from CoPc at 800 and 900 °C and NiPc at 850, 900, and 1000 °C. The respective notation is given as Co-800, Co-900, Ni-850, Ni-900, and Ni-1000.

The XPS measurements were performed at the U7 beam line of the Pohang Light Source (PLS). The U7 beam line was designed to provide soft X-rays in the energy range of 50−1500 eV.[30] The XPS data were collected using four photon energies 360, 475, 625, and 1265 eV, with the photon flux of $\sim 7 \times 10$,[11] $\sim 6 \times 10$,[11] $\sim 4 \times 10$,[11] and $\sim 3 \times 10^{10}$ (photons/s/200mA), respectively. The binding energies were corrected for specimen charging by referencing the C 1s peak to 284.6 eV, and the background was subtracted by Shirley's method.[31] The experiment was performed in an ultrahigh vacuum (UHV) chamber with a base pressure $\leq 5 \times 10^{-10}$. The photoelectrons emitted from the surface of the N-doped CNTs were collected and their energy was analyzed with an electron energy analyzer (Physical Electronics: Model PHI 3057 with a 16-channel detector). The analyzer was located at 55° from the surface normal. The binding energy was calibrated by using the C 1s peak (284.6 eV). The XPS peak was curve-fitted by Voigt profiles.

The XANES measurement was performed at the U7 beam line of PLS. The spectral resolving power ($E/\Delta E$) of the incident photon is about 5000 at 400 eV. All spectra were taken in a total electron yield mode recording the sample current at room temperature. The photon energy was calibrated by the second peak in the π^* resonance of N_2 gas to be 401.1 eV as a reference. To eliminate the effect of incident beam intensity fluctuations and monochromator absorption features, all spectra were normalized by a reference signal from an Au mesh with 90% transmission. The EELS (GATAN GIF-2000) attached to TEM (FEI TECNAI G^2) was used to provide the electronic states of N atoms in individual nanotube.

3. Results

3.1. Structure and Crystallinity. We have previously explained the detailed configuration and structural characteristics of CNTs in ref 29. Figure 1a shows the SEM image for the vertically aligned CNTs grown using FePc at 900 °C (Fe-900). TEM image shows the general morphology of CNTs (Figure 1b). They exhibit a typical bamboo-like structure. The average diameter is 20 nm, and the wall thickness is about 5 nm. Figure 1c corresponds to the TEM image for the CNTs grown using CoPc at 900 °C (Co-900). The average diameter and wall thickness are 30 and 8 nm, respectively. The TEM image of CNTs grown using NiPc at 900 °C (Ni-900) shows the average diameter 50 nm and the wall thickness 20 nm, which are more than 2-times larger than those of Fe-900 (Figure 1d). The outer diameter and wall thickness of all CNTs are listed in Table 1, showing that both of them increase with the growth temperature. The morphology of CNTs grown using CoPc is similar with that of CNTs grown using FePc at the same growth temperature. The diameter is in the range 15−50 nm, and the wall thickness is 5−8 nm. But the wall thickness of CNTs grown using NiPc is about 3−5 times larger than those of CNTs grown using FePc or CoPc at the same growth temperature.

TABLE 1: The N Atomic % Measured by XPS Using Three Photon Energies 475, 625, and 1265 eV

source	temp. (°C)	sample no.	dia. (nm)	wall thick. (nm)	I_D/I_G[a]	$h\nu$ (eV)	N content (at. %) 475	625	1265	ave.[b]
FePc	750	Fe-750	15	5	0.77		2.6	4.5	6.0	4.3
	850	Fe-850	20	5	0.74		1.6	2.4	3.2	2.4
	900	Fe-900	20	5	0.67		1.5	2.5	5.6	3.2
	1000	Fe-1000	50	8	0.62		0.8	1.6	2.6	1.7
CoPc	800	Co-800	20	5	0.72		0.7	2.1	3.3	2.1
	900	Co-900	30	8	0.66		0.8	1.7	2.5	1.7
NiPc	850	Ni-850	40	15	0.82		1.7	4.2	7.8	4.6
	900	Ni-900	50	20	0.73		1.4	2.9	5.5	3.3
	1000	Ni-1000	80	40	0.70		1.5	2.7	4.1	2.8

[a] The intensity ratio of D band relative to G band of Raman spectrum with an error of 5%. [b] The average value of N at. % measured using three photon energies 475, 625, and 1265 eV.

Raman spectroscopy was employed in order to obtain the information about the crystallinity of entire CNTs. The first-order spectrum consists of two bands at ~ 1580 cm^{-1} (G band) and ~ 1350 cm^{-1} (D band) that are originated from the Raman active in-plane atomic displacement E_{2g} mode and disorder-induced features due to the finite particle size effect or lattice distortion, respectively.[32] The intensity ratio of D band to G band (I_D/I_G) has a linear relation with the inverse of the in-plane crystallite dimension. The I_D/I_G value of all samples is listed in Table 1, showing an increase of the crystallinity with the growth temperature. Over the temperature range, the degree of crystalline perfection is always lower for the CNTs grown using NiPc than those of CNTs grown using FePc and CoPc.

3.2. N Atom Concentration. We measured the XPS using three photon energies 475, 625, and 1265 eV. The respective probing depth of N 1s electrons is estimated to be about 1, 2, and 5 nm.[28] Figure 2 shows the XPS survey scan spectrum of Fe-750, Fe-900, and Fe-1000. The XPS data show distinct C, N, and O 1s peaks. The O 1s peak cannot be detected at 475 eV that is below the threshold energy. The O peak would be originated mainly from the substrates, with some contribution from the dangling bonds of graphite layers such as C═O. The N concentration, defined as N/(C + N) atomic ratio %, was estimated by the area ratio of the N 1s and C 1s peaks, taking into consideration of their relative sensitivities. As the photon energy increases from 475 to 1265 eV, the N % increases from 2.6% to 6.0% for Fe-750, from 1.5% to 5.6% for Fe-900, and from 0.8% to 2.6% for Fe-1000. The N % increase corresponds to a factor of 2−3 as the probing depth increases from 1 to 5 nm, indicating the higher N content in the more inside parts of nanotubes. Such N % increase with the photon energy can be also observed from the CNTs grown using CoPc and NiPc, as listed in Table 1. The average value of N % is obtained from

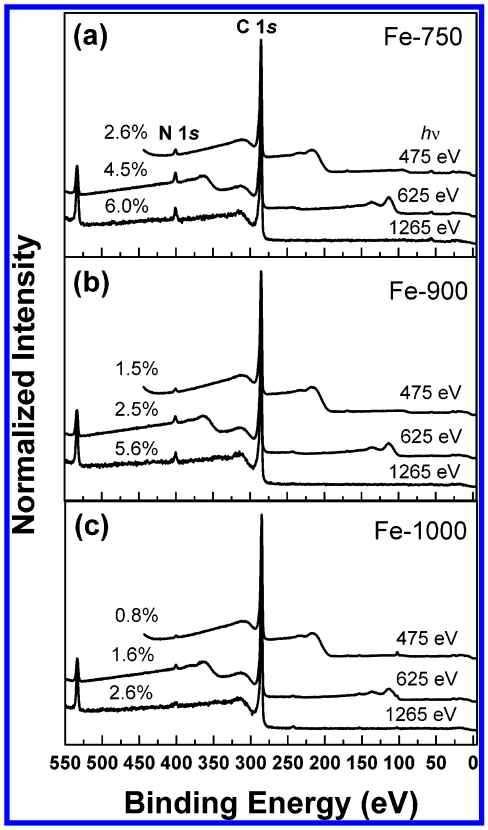

Figure 2. XPS survey scan spectrum measured using three photon energies 475, 625, and 1265 eV for (a) Fe-750, (b) Fe-900, and (c) Fe-1000. As the photon energy increases from 475 to 1265 eV, N % increases from 2.6% to 6.0% for Fe-750, from 1.5% to 5.6% for Fe-900, and from 0.8% to 2.6% for Fe-1000.

the values measured using three photon energies, showing a decrease as the growth temperature increases. This result is quite consistent with recent work of Tang et al. using the pyrolysis of dimethylformide at 650−1175 °C.[24] The averaged N % of Fe-900 and Ni-900 is nearly the same, although the crystallinity of Fe-900 is better than that of Ni-900.

3.3. Electronic Structure of C and N Atoms. To get the electronic structure of C and N atoms, we obtained the respective fine-scanned C 1s and N 1s peaks. We used the photon energy 360, 625, and 1265 eV for C 1s, to compare the electronic structure at the similar probing depth as that of N 1s.[28] The C 1s spectrum of Fe-900 is displayed in Figure 3a. For all three photon energies, it shows an asymmetric band centered at 284.6 eV. From the curve fitting, the band can be deconvoluted into three bands at 284.5 (PC1), 285.5 (PC2), and 287 eV (PC3). It is expected that the binding energy of C atoms bonded to the N atoms will appear at a higher energy compared to those of pure graphite C atoms due to the higher electronegativity of N atoms. Therefore the strongest PC1 can be assigned to the C atoms binding to C atoms, and the weaker PC2 corresponds to the C atoms binding to N atoms. This assignment is consistent with the previous works of CN_x films.[33] We ascribe the weakest PC3 to the other binding configurations such as C═O or C≡N that can be formed at the edge of graphite layers. The area % of PC1, PC2, and PC3 is 75, 17, and 8 at 360 eV; 74, 20, and 6 at 625 eV; 74, 21, and 5 at 1265 eV, respectively. As the photon energy increases, the fraction of N-bonded structure PC2 tends to increase while that of graphite structure PC1 and other structure PC3 decreases. It indicates the higher N concentration at the more inside parts of nanotubes. The area % of PC1, PC2, and PC3 for all samples is listed in Supporting Information (Table S1).

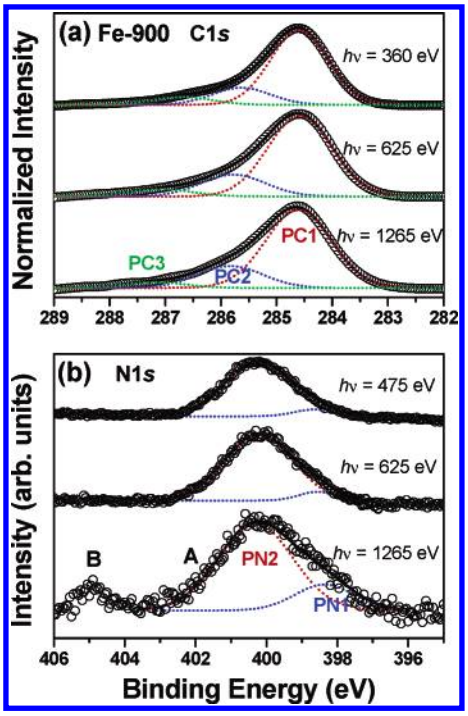

Figure 3. (a) The C 1s XPS spectrum of Fe-900 using 360, 625, and 1265 eV. The data points (open circles) of C 1s band are fitted by three Voigt functions PC1, PC2, and PC3 (dotted lines). As the photon energy increases, the fraction of N-bonded structure PC2 tends to increase while that of graphite structure PC1 and other structure PC3 decreases. (b) The N 1s is XPS spectrum of Fe-900 using 475, 625, and 1265 eV. The data points (open circles) of N 1s band (labeled as A) are fitted by two Voigt functions PN1 and PN2 (dotted lines). The sum of deconvoluted bands is marked by lines. The area % of PN1 (pyridine-like) and PN2 (graphite-like) bands is 7 and 93 at 475 eV; 7 and 93 at 625 eV; 19 and 81 at 1265 eV. A new band (labeled as B) corresponding to molecular N_2 appears at 405.0 eV.

Figure 3b displays the N 1s XPS spectrum of Fe-900, showing a band (labeled as A) centered at 400.5 eV. The asymmetric shape suggests at least two main components, so the band has been deconvoluted into two bands at 398.4 (PN1) and 400.2 eV (PN2). The peak assignment of N 1s diverges somewhat between different authors. In the CN_x films, the peaks at lower and higher binding energies were assigned to the N atoms bonded to sp^3 (or C_3N_4) and sp^2 hybridized carbon, respectively, by a number of research groups.[34−38] Recently, the same assignment were performed for the N-doped CNTs.[23] However, since the N content of the present CNTs is less than 10%, we assign these bands to the sp^2 hybridized N atoms such as pyridine-like and graphite-like structures, respectively, following the assignment of low-concentration N containing CN_x film.[11,14] Our assignment is consistent with the previous work of other groups on the N-doped CNTs.[19,20,22] The area % of PN1 (pyridine-like) and PN2 (graphite-like) is 7 and 93 at 475 eV; 7 and 93 at 625 eV; 19 and 81 at 1265 eV, respectively, as listed in Table 2. It shows that the graphite-like N structure is more abundant than the pyridine-like N structure. But as the photon energy increases, the fraction of the pyridine-like N structure increases by more than 2 times.

When 1265 eV is used, a new band (labeled as B) appears at 405.0 eV, indicating that another electronic structure of N atoms appears at the inner parts. We assign this band to the molecular N_2 by following reason. The N 1s binding energy is 409.9 eV for free N_2 gas,[39] but the energy becomes lowered if there is

TABLE 2: Area % of Deconvoluted Bands from the N 1s Peak for the CNTs Grown via the Pyrolysis of FePc, CoPc, and NiPc at Various Temperatures

source	sample no.	photon energy (eV)	area % of deconvoluted band			
			PN1	ave.	PN2	ave.
FePc	Fe-750	475	15	18	85	82
		625	16		84	
		1265	23		77	
	Fe-800	475	12	15	88	85
		625	12		88	
		1265	20		81	
	Fe-900	475	7	11	93	89
		625	7		93	
		1265	19		81	
	Fe-1000	475	6	8	94	92
		625	8		92	
		1265	11		89	
CoPc	Co-800	475	9	11	91	89
		625	12		88	
		1265	13		87	
	Co-900	475	5	7	95	93
		625	7		92	
		1265	9		91	
NiPc	Ni-850	475	49	53	51	47
		625	51		49	
		1265	59		41	
	Ni-900	475	27	36	73	64
		625	34		66	
		1265	48		52	
	Ni-1000	475	38	34	62	66
		625	35		65	
		1265	30		70	

extra-atomic screening effect between N 1s core hole and matrix. The energy lowering was observed from a number of systems; the interstitial N_2 on TiAlN (403.2 eV), physisorbed N_2 on W (403.3 eV) and graphite (403.9 eV), and chemisorbed N_2 on Re (405.2 eV) and W (405.3 eV).[40−42] Considering the possible energy position of the band B and the probing depth (about 5 nm) of N 1s photoelectrons at 1265 eV, molecular N_2 would exist at the interstitial and/or intercalated sites between the graphite layers near to the hollow inside. Since the graphite layers are in a highly ordered crystalline structure as shown in the HRTEM images, the molecular N_2 would exist preferentially as an intercalated form.

Figure 4a displays the N 1s XPS spectrum of Co-900. The band was deconvoluted into two bands PN1 and PN2. The area % of PN1 (pyridine-like) and PN2 (graphite-like) is 5 and 95 at 475 eV; 8 and 92 at 625 eV; 9 and 91 at 1265 eV, respectively. The area % of graphite-like N structure PN2 is larger than the case of Fe-900, due to a less N content. Figure 4b displays the N 1s XPS spectrum of Ni-900. The area % of PN1 and PN2 is 27 and 73 at 475 eV; 34 and 66 at 625 eV; 48 and 52 at 1265 eV, respectively. The fraction of pyridine-like N structure is more significant than the case of Fe-900. The higher fraction of pyridine-like N structure with the higher photon energy is consistent with the case of Fe-900 and Co-900. The graphite-like and pyridine-like N structures exist with the nearly same amount at around 5 nm from the surface of nanotubes. This higher content of pyridine-like N structure could be correlated with the lower degree of crystalline perfection compared to that of Fe-900. These Co-900 and Ni-900 do not show any detectable molecular N_2 band.

The XPS has been measured for all other samples, showing at least a trace of molecular N_2 band for Fe-750, Fe-800, Fe-900, and Co-800, only when the photon energy is 1265 eV. These samples have a common property that the average wall thickness is 5 nm. Since the estimated probing depth is 5 nm at 1265 eV, the N_2 signal would come from the vicinity of hollow

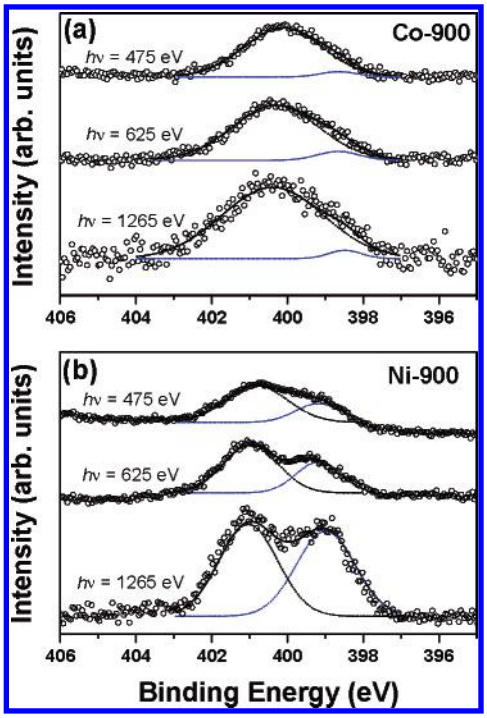

Figure 4. The N 1s is XPS spectrum of (a) Co-900 and (b) Ni-900, using 475, 625, and 1265 eV. The data points (open circles) of N 1s band are fitted by two Voigt functions PN1 and PN2 (dotted lines). The sum of deconvoluted bands is marked by lines. The area ratio of PN1 (pyridine-like)/PN2 (graphite-like) bands increases at the higher photon energy.

inside. Table 2 lists the area % of PN1 and PN2 bands deconvoluted from N 1s band, for all CNTs grown using FePc, CoPc, and NiPc. The fraction of PN1 (pyridine-like structure) always increases as going inside from the surface. The pyridine-like N structure of the CNTs grown using FePc and CoPc takes much less fraction than that of the CNTs grown using NiPc for all temperatures. The average value is obtained from the values measured using three photon energies. As the growth temperature increases, the average fraction of pyridine-like N structure always decreases. We conclude that the fraction of pyridine-like N structure determines the degree of crystalline perfection of CNTs.

3.4. Valence Band Structure. To investigate the N-doping effect on the nature of band structure, we obtained the valence band (VB) using the photon energy 360 eV. The zero energy is chosen at the Fermi level, E_f, which is the threshold of the emission spectrum. The valence band electrons are responsible for bonding and thus significant change in the density of states (DOS). Figure 5a displays the valence band of XPS for Fe-750, Fe-900, and Fe-1000. Figure 5b displays the valence band spectrum for Co-800 and Co-900. Figure 5c corresponds to the spectrum of Ni-850, Ni-900, and Ni-1000. The spectrum is normalized using the intensity at 13 eV. Following the works of CN_x films, the spectrum is separated into two distinct regions; region A at 0−6.5 eV and region B at 6.5−12 eV, which attributes to C 2p and N 2p electrons associated to π bonds in graphite structure and N lone-pair electrons, and to C 2 p and N 2 p electrons associated with σ bonds, respectively.[35,43]

In the case of the CNTs grown using FePc, as the content of pyridine-like structure increases (as the temperature decreases), the overall intensity enhances with more influenced region A. The similar enhancement of region A is also observed from the CNTs grown using CoPc, despite of the ambiguous spectral feature due to a less N content. The curve of region A of Co-

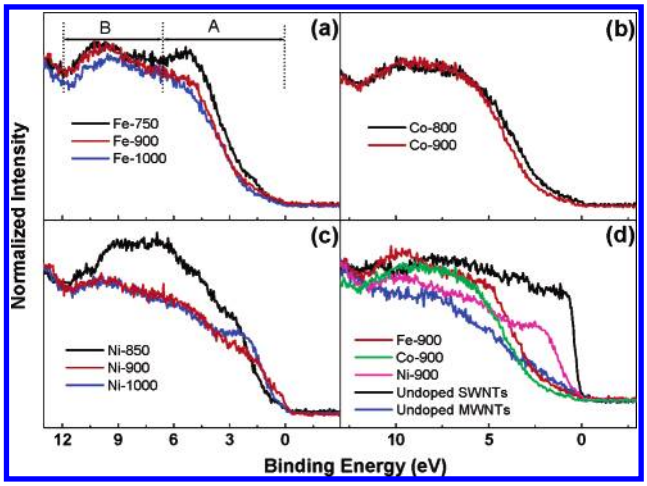

Figure 5. Valence band of XPS using 360 eV for (a) Fe-750, Fe-900, and Fe-1000; (b) Co-800 and Co-900; (c) Ni-850, Ni-900, and Ni-1000; (d) Fe-900, Co-900, Ni-900, undoped SWNTs synthesized via arc-discharge, and undoped MWNTs synthesized via CVD. The spectrum consists of two regions: region A at 0−6.5 eV and region B at 6.5−12 eV.

800 is nearly overlapped with that of Fe-900. For the CNTs grown using NiPc, as the N content increases, the intensity above 2.5 eV increases whereas the intensity at 1−2.5 eV decreases. Chen et al. reported that the intensity of region A can increase as the crystallinity of graphite sheets of CN_x film increases.[43] They interpret the result by the increase of 2 p electrons in C−C π bonds. In contrast, Suzuki et al. reported that the tips of MWNTs exhibit a lager intensity than the sidewalls, due to the DOS of dangling bond.[44,45] The higher content of pyridine-like structure results in the enhanced A region, mainly due to the larger numbers of lone-pair electron of N atoms formed at the dangling bonds. The decreased intensity at 1−2.5 eV (Ni-850) would be related with the deteriorated crystallinity due to the large amount of pyridine-like structure.

The spectrum of Fe-900, Co-900, and Ni-900 has been compared with that of undoped SWNTs synthesized via arc-discharge and undoped MWNTs synthesized via CVD and (Figure 5d).[46] The average N content of Fe-900, Co-900, and Ni-900 is 3.2%, 1.7%, and 3.3%, and the average % fraction of pyridine-like N structure is 11, 7, and 36, respectively. It definitely shows that the higher content of pyridine-like N structure induces the higher DOS in the vicinity of E_f. The vertical rise of metallic SWNTs at the zero E_f indicates a nearly perfect metallic nature. The undoped MWNTs show a much slower rise corresponding to more semiconductor nature. It indicates that the more metallic behavior can be induced by the higher content of pyridine-like N structure.

3.5. XANES of N Atoms. Figure 6 shows the N K-edge XANES spectrum of all CNTs. It consists of three features centered at 399, 401, and 408 eV, labeled as A, B, and C, respectively. It is well-known that the transitions from 1s into unoccupied π^* orbitals of pyridine-like and graphite-like N structures of CN_x film usually appear at 398.3 and 400.7 eV, respectively.[13,14] Therefore, the A and B features are assigned to the π^* features of pyridine-like and graphite-like N structures, respectively. The broad C feature can be assigned to the transitions from 1s into unoccupied σ^* orbitals.

In the case of CNTs grown using NiPc (Figure 6c), the relative intensity of A/B peaks decreases with the growth temperature, indicating the less fraction of pyridine-like N structure for the less N-containing CNTs. This result is consistent with the XPS results. Surprisingly intense B feature is observed

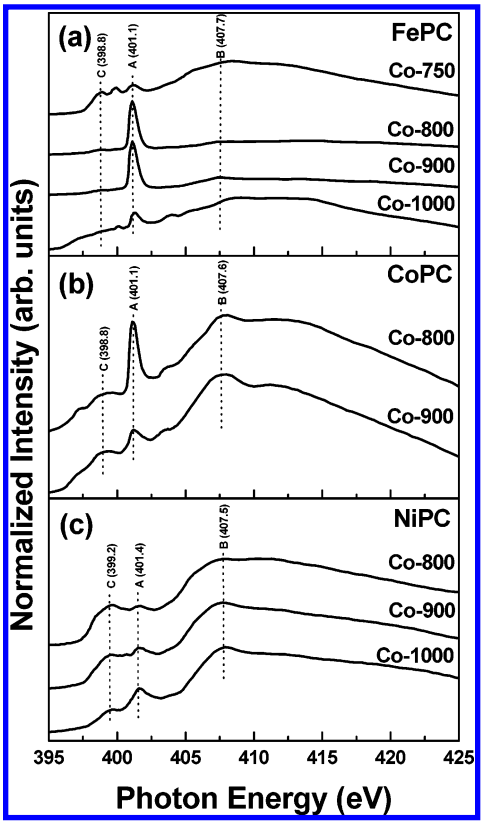

Figure 6. N K-edge XANES spectrum showing three major features centered at 399 (labeled as A, π^* of pyridine-like), 401 (labeled as B, π^* of graphite-like and molecular N_2), and 408 eV (labeled as C, σ^*).

from Fe-800, Fe-900, and Co-800, indicating the existence of another N structure (Figure 6a and Figure 6b). Following the XPS data showing the presence of molecular N_2 from these samples, we suggest that the π^* feature of molecular N_2 peaks may superimpose on that of graphite-like N structure. The π^* feature of free N_2 gas exhibits a vibrational fine structure at the same position.[30,42] We actually observed that the B feature splits into the vibrationally resolved fine structure in the higher N-concentration CNTs (Supporting Information, Figure S1). The lack of vibrational splitting feature implies that the π^* level of molecular N_2 would be highly perturbed by surrounding matrix. It is most likely that the intercalation of molecular N_2 between the graphite layers takes place. The XANES technique using the sample current mode can give more averaged information on the electronic structure of CNTs due to the longer probing depth than XPS, which is estimated to be higher than 10 nm.[47,48] The notable detection of molecular N_2 peak can be rationalized by the longer probing depth than the wall thickness.

3.6. EELS Data Showing the Encapsulated N_2. Figure 7 shows the EELS spectrum for the edge and center parts of an Fe-900 CNT whose EELS (or energy-filtered TEM) imaging is shown in the inset. The N elemental mapping uses the energy loss of K-shell edges of N (ΔE = 400 eV). The brighter points represent a higher concentration of the element, showing that the N components exist concentrated at the inner walls and the compartment region. A detailed inspection of the near-edge fine structure confirms the sp^2 hybridization state for C, distinguished by a sharply defined π^* at 288 eV and a broad σ^* feature. The edge part exhibits the N−K edge feature incorporated into sp^2-graphite frameworks; π^* peak at 399 eV and a broad σ^* feature. In contrast, the center part shows the remarkably different N−K edge feature that a strong peak of N_2 at 401 eV overlaps on the π^* peak (399 eV), which is very consistent with the N_2 peak

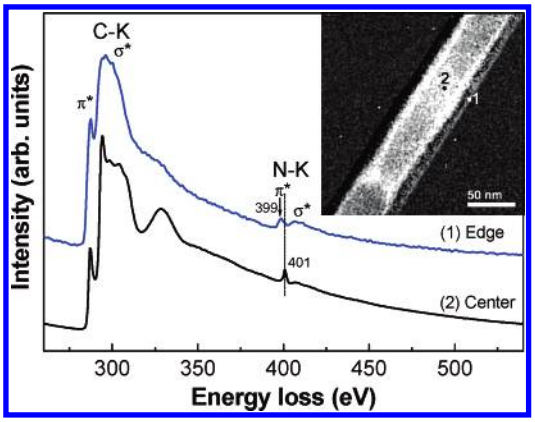

Figure 7. The EELS spectrum of the (1) edge and (2) center parts of an Fe-900 CNT, showing the N_2 peak at 401 eV. Inset corresponds to its elemental map of N atoms, obtained by EELS imaging using inelastic electrons corresponding to the energy loss of N−K edge.

feature previously reported by other research groups.[17,18,24] These data undoubtedly indicates that molecular N_2 exists inside the nanotubes, dominantly as the intercalated and trapped forms. The N at. % is determined to be about 10, which is close to the N content measured by XPS. The depletion of N_2 via heating has been observed and will be reported in a following paper.

4. Discussion

We observed that the CNTs are doped with N atoms, with the following properties that (1) the more inside parts of CNTs contains the higher N atom concentration up to 8%; (2) three different N structures such as graphite-like, pyridine-like, and molecular N_2 exist; (3) the pyridine-like N structure and molecular N_2 become significant at the inner parts; (4) molecular N_2 could present as intercalated form in the inner walls. These results have been proved systematically using the core-level electron absorption of C and N atoms. The variable photon energy of XPS provides the opportunities to examine the electronic structure depending on the probing depth. This advantage of the variable-energy XPS has been recently used for the structure analysis of surface.[49,50] The synchrotron X-ray source with high photon flux enables to resolve the N 1s spectrum with a high reliability. The high-resolution N 1s XPS data reveals clearly three different-typed electronic structures of N atoms. The XANES offers a rigorous supporting data for the presence of three N structures due to the longer probing depth than XPS. The EELS provides the electronic states of N atoms in individual nanotube although the resolution is lower than the XPS and XANES. Combining of XPS, XANES, and EELS provides the remarkable and surprising conclusion that the relative ratio of three N structures depends on the distance from the surface of CNTs. We believed that such inhomogeneous N-doping takes places for all MWNTs.

The N-doping in the inner wall is more favorable than that in the outer wall for both graphite-like and pyridine-like N structures. Due to the deficiency of C atoms, the pyridine-like N structure would exhibit more flexibility than the graphite-like N structure, so it can release more efficiently the strains of curved graphite layers intrinsically occurring in the nanotubes. If the N atoms dope in the smaller-diameter walls, the strain-releasing effect would be larger. The incorporation of N atoms preferentially in the inner walls of MWNTs would be thus thermodynamically driven during the growth. This explains why the formation of pyridine-like N structure takes place favorably at the inner walls. The defects at the inner wall are also favorable than the outer wall in the same context.

Because of the deficiency of atoms, as we described above, the content of pyridine-like structure must have a strong correlation with the degree of crystalline perfection. We previously reported that as the N content increases, the degree of crystalline perfection decreases.[27,29] In addition, the N-doping promotes the production of bamboo-like structure by facilitating the joint of the wall and compartment layers due to the enhanced flexibility. These all are based on the assumption that the content of pyridine-like structure is proportional to the N content. Here we can justify the assumption by analyzing the content of three different N structures. Terrones and co-workers also reported that as the N content increases, the pyridine-like N structures become dominant to the graphite-like N structures and the nanotubes becomes less straight with reduced mechanical properties, which is consistent well with our results.[51]

One noble finding is the molecular N_2 that would exist as an intercalated form between the walls in the vicinity of hollow inside. The N_2 molecules could be generated in gas phase by the pyrolysis reaction of Pc molecules or by the precipitation from the N-dissolved metal catalytic particles, and then be intercalated or trapped during the growth of CNTs. The molecular N_2 peak is found in the CNTs grown using FePc and CoPc, probably due to their wall thickness less than the probing depth. If the probing depth of XPS and XANES is long enough to examine the more inside of the thick CNTs grown using NiPc, the peaks of molecular N_2 could be detected. The trapped form of molecular N_2 inside the compartments probably takes place for all CNTs.

There is a significant difference between the CNTs grown using NiPc and FePc (or CoPc). The CNTs grown using NiPc have the larger diameter and wall thickness compared to those of FePc and CoPc, and they also contain much higher concentration of pyridine-like N structure than the others. So the question arises, Why does the NiPc exhibit a unique behavior? To find the reason, let us conjecture the growth mechanism of the present N-doped CNTs. The closed tip without the capped catalytic particles indicates that the CNTs would be grown out from the catalytic particles deposited on the substrates. The growth mechanism follows a typical base-growth mechanism, which is consistent with that of other research groups.[52,53] The diameter and wall thickness of nanotubes usually increases with the temperature, since the average size of catalytic nanoparticles increases due to the more efficient agglomeration of nanoparticles on the surface of substrates. The larger diameter and wall thickness of the CNTs grown using NiPc are also related with the larger Ni nanoparticles than Fe or Co nanoparticles.

Our group proposed that the bulk diffusion of C atoms plays an important role in determining the growth rate and the structure, based on the temperature-dependent growth rate of CNTs.[27,29] The growth rate is mainly proportional to the saturated concentration and bulk diffusion rate of C atoms in metal. We suggested that the higher saturated concentration of N atoms in metal would produce the more N-doped graphite sheets. According to the available phase diagram, the saturated N concentration is 25 at. % in Ni, while only 10 at. % in γ-Fe at 700 °C.[54] This may explain the more abundant pyridine-like N structure in the CNTs grown using NiPc. The less pyridine-like N content at the higher temperature could be related with the faster increase of the build-up rate of C atoms than that of N atoms. It is known that the saturated concentration of N atoms in γ-Fe decreases from 10 to 8 at. % as the temperature increases from 700 to 900 °C, which is opposite to the saturated C atoms.[54] But since no further data are available, we cannot provide a

definite explanation for the dependence of pyridine-like N content on the temperature and catalyst.

As shown in the valence band of XPS, the pyridine-like N structure is responsible for the metallic behavior, which is consistent with the result of Terrones group.[10] The present work reveals that the level of metallic properties can be controlled by the content of pyridine-like N structure. Since the existence of molecular N_2 contributes in increasing the N content, the higher N content cannot guarantee the higher content of pyridine-like N structure. This finding suggests that the control of the pyridine-like N content rather than the N content would be imperative in the fabrication of metallic typed CNTs. Finally, the results show that the content of pyridine-like N structure can be manipulated by the reactant and growth temperature. These N-doped CNTs can be a huge nanosize container for the N atoms as chemically bonding form or N_2 gas.

5. Conclusion

The N-doped CNTs were grown by pyrolyzing FePc, CoPc, and NiPc in the temperature range 750−1000 °C. The CNTs usually have a bamboo-like structure. The diameter and wall thickness of CNTs grown using FePc and CoPc is 15−50 and 5−8 nm, respectively, but the CNTs grown using NiPc have more than 2-times larger diameter and wall thickness. The concentration and electronic structure of the doped N atoms were intensively examined by XPS, XANES, and EELS.

As the photon energy of XPS varies from 475 to 1265 eV, the N content increases up to 8%, indicating a higher N concentration at the more inside parts of nanotubes. The deconvolution of N 1s peak reveals three different N structures that are graphite-like, pyridine-like, and molecular N_2. The pyridine-like structure becomes important at the inner walls. The molecular N_2 peak was detected in the CNTs grown using FePc and CoPc whose wall thickness is at least comparable to the probing depth. The peak feature suggests the existence of molecular N_2 as intercalated form in the vicinity of hollow inside. The XANES and EELS data provide evidence that molecular N_2 exists inside the nanotubes, dominantly as the intercalated and trapped forms. The CNTs grown using NiPc contain the higher concentration of pyridine-like N structure than those grown using FePc and CoPc. The higher content of pyridine-like N structure would lead more metallic behaviors of CNTs. It is also responsible for the deterioration of the crystallinity of CNTs. The pyridine-like N structure becomes more significant in the inner wall than that of graphite-like structure, which can be justified by the strain release of the graphite sheets. The dependence of pyridine-like N content on the CNTs has been tentatively explained by the growth mechanism, showing that the control of pyridine-like N content can be achieved by the growth conditions.

Acknowledgment. This work was supported by KOSEF (Project No. R14-2004-033-01003-0 and R02-2004-000-10025-0) and KRF (Project No. 2004-015-C00265). B.K. thanks MOST for National R&D Project for NT. SEM analyses were performed at Basic Science Research Center in Seoul. Experiments at PLS were supported in part by MOST and POSTECH.

Supporting Information Available: Area % of deconvoluted bands from the C 1s peak, and high-resolution N K-edge XANES spectrum showing the vibrationally resolved π^* resonance peaks for the N-doped CNTs grown using FePc at 900 °C. This material is available free of charge via the Internet at http://pubs.acs.org.

References and Notes

(1) Treacy, M. M. J.; Ebbesen, T. W.; Gibson, J. M. *Nature* **1996**, *381*, 678.

(2) Odom, T. W.; Huang, J.-L.; Kim, P.; Lieber, C. M. *Nature* **1998**, *391*, 62.

(3) Saito, Y.; Hamaguchi, K.; Hata, K.; Uchida, K.; Tasaka, Y.; Ikazaki, F.; Yumura, M.; Kasuya, A.; Nishina, Y. *Nature* **1997**, *389*, 554.

(4) Fan, S.; Chapline, M. G.; Franklin, N. R.; Tombler, T. W.; Cassell, A. M.; Dai, H. *Science* **1999**, *283*, 512.

(5) Tans, S. J.; Alwin, R. M.; Verschueren, A. R. M.; Dekker, C. *Nature* **1998**, *393*, 49.

(6) Rueckes, T.; Kim, K.; Joselevich, E.; Tseng, G. Y.; Cheung, C.-L.; Lieber, C. M. *Science* **2000**, *289*, 94.

(7) Bachtold, A.; Hadley, P.; Nakanishi, T.; Dekker, C. *Science* **2001**, *294*, 1317.

(8) Liang, W.; Bockrath, M.; Bozovic, D.; Hafner, J. H.; Tinkham, M.; Park, H. *Nature* **2001**, *411*, 665.

(9) Hamada, S.; Sawada, S.; Oshiyama, A. *Phys. Rev. Lett.* **1992**, *68*, 1579.

(10) (a) Czerw, R.; Terrones, M.; Charlier, J.-C.; Blase, X.; Foley, B.; Kamalakaran, R.; Grobert, N.; Terrones, H.; Tekleab, D.; Ajayan, P. M.; Blau, W.; Rühle, M.; Carroll, D. L. *Nano Lett.* **2001**, *1*, 457. (b) Terrones, M.; Ajayan, P. M.; Banhart, F.; Blase, X.; Carroll, D. L.; Charlier, J. C.; Czerw, R.; Foley, B.; Grobert, N.; Kamalakaran, R.; Kohler-Redlich, Ph.; Rühle, M.; Seeger, T.; Terrones, H. *Appl. Phys. A* **2002**, *74*, 355.

(11) Casanovas, J.; Ricart, J. M.; Rubio, J.; Illas, F.; Jiménez-Mateos, J. M. *J. Am. Chem. Soc.* **1996**, *118*, 8071.

(12) Ripalda, J. M.; Román, E.; Díaz, N.; Galán, L.; Montero, I.; Comelli, G.; Baraldi, A.; Lizzit, S.; Goldoni, A.; Paolucci, G. *Phys. Rev. B* **1999**, *60*, R3705.

(13) Shimoyama, I.; Wu, G.; Sekiguchi, T.; Baba, Y. *Phys. Rev. B* **2000**, *62*, R6053.

(14) Shimoyama, I.; Wu, G.; Sekiguchi, T.; Baba, Y. *J. Electron Spectrosc. Relat. Phenom.* **2001**, *114*−*116*, 841.

(15) dos Santos, M. C.; Alvarez, F. *Phys. Rev. B* **1998**, *58*, 13918.

(16) Miyamoto, Y.; Cohen, M. L.; Louie, S. G. *Solid State Commun.* **1997**, *102*, 605.

(17) Terrones, M.; Kamalakaran, R.; Seeger, T.; Rühle, M. *Chem. Commun.* **2000**, 2335.

(18) Trasobares, S.; Stéphan, O.; Colliex, C.; Hug, G.; Hsu, W. K.; Kroto, H. W.; Walton, D. R. M. *Eur. Phys. J. B.* **2001**, *22*, 117.

(19) Sen, R.; Satishkumar, B. C.; Govindaraj, A.; Harikumar, K. R.; Renganathan, M. K.; Rao, C. N. R. *J. Mater. Chem.* **1997**, *7*, 2335.

(20) Terrones, M.; Redlich, P.; Grobert, N.; Trasobares, S.; Hsu, W. K.; Terrones, H.; Zhu, Y. Q.; Hare, J. P.; Reeves, C. L.; Cheetham, A. K.; Rühle, M.; Kroto, H. W.; Walton, D. R. M. *Adv. Mater.* **1999**, *11*, 655.

(21) Wang, X.; Liu, Y.; Zhu, D.; Zhang, L.; Ma, H.; Yao, N.; Zhang, B. *J. Phys. Chem. B* **2002**, *106*, 2186.

(22) Kudashov, A. G.; Okotrub, A. V.; Bulusheva, L. G.; Asanov, I. P.; Shubin, Yu. V.; Yudanov, N. F.; Yudanova, L. I.; Danilovich, V. S.; Abrosimov, O. G. *J. Phys. Chem. B* **2004**, *108*, 9048.

(23) Jang, J. W.; Lee, C. E.; Lyu, S. C.; Lee, T. J.; Lee, C. J. *Appl. Phys. Lett.* **2004**, *84*, 2877.

(24) Tang, C.; Bando, Y.; Golberg, D.; Fu, F. *Carbon* **2004**, *42*, 2625.

(25) Han, W. Q.; Redlich, P.; Seeger, T.; Ernst, F.; Rühle, M.; Grobert, N.; Hsu, W. K.; Chang, B. H.; Zhu, Y. Q.; Kroto, H. W.; Walton, D. R. M.; Terrones, M.; Terrones, H. *Appl. Phys. Lett.* **2000**, *77*, 1807.

(26) Suenaga, K.; Yudasaka, N.; Colliex, C.; Iijima, S. *Chem. Phys. Lett.* **2000**, *316*, 365.

(27) Lee, Y. T.; Kim, N. S.; Bae, S. Y.; Park, J.; Yu, S.-C.; Ryu, H.; Lee, H. J. *J. Phys. Chem. B* **2003**, *107*, 12958.

(28) Teo, B. K. *EXAFS: Basic Principles and Data Analysis*; Springer-Verlag: Berlin, 1986; p 92.

(29) Kim, N. S.; Lee, Y. T.; Park, J.; Han, J. B.; Choi, Y. S.; Choi, S. Y.; Choo, J.; Lee. G. H. *J. Phys. Chem. B* **2003**, *107*, 9249.

(30) Lee, M. K.; Shin, H.-J. *Nucl. Instrum. Methods Phys. Rev. A* **2001**, *467*−*468*, 508.

(31) Shirley, D. A. *Phys. Rev. B* **1972**, *5*, 4709.

(32) Tuinstra, F.; Koenig, J. L. *J. Chem. Phys.* **1970**, *53*, 1126.

(33) Beshkov, G.; Dimitrov, D. B.; Georgiev, St.; Juan-Cheng, D.; Petrov, P.; Velchev, N.; Krastev, V. *Diamond Relat. Mater.* **1999**, *8*, 591.

(34) Marton, D.; Boyd, K. J.; Al-Bayati, A. H.; Todorov, S. S.; Rabalais, J. W. *Phys. Rev. Lett.* **1994**, *73*, 118.

(35) Souto, S.; Pickholz, M.; dos Santos, M. C.; Alvarez, F. *Phys. Rev. B.* **1998**, *57*, 2536.

(36) Hellgren, N.; Johansson, M. P.; Broitman, E.; Hultman, L.; Sundgren, J.-E. *Phys. Rev. B.* **1999**, *59*, 5162.

(37) Johansson, Å.; Stafström, S. *J. Chem. Phys.* **1999**, *111*, 3203.

(38) Ohta, R.; Lee, K. H.; Saito, N.; Inoue, Y.; Sugimura, H.; Takai, O. *Thin Solid Films* **2003**, *434*, 296.

(39) Brundle, C. R. *J. Vac. Sci. Technol.* **1976**, *13* 301.
(40) Grunze, M. J.; Fuhler, J.; Neumann, M.; Brundle, C. R.; Auerbach, D. J.; Behm, J. *Surf. Sci.* **1984**, *139*, 109.
(41) Björneholm, O.; Nilsson, A.; Sandell, A.; Hernnäs, B.; Mårtensson, N. *Phys. Rev. Lett.* **1992**, *68*, 1892.
(42) Esaka, F.; Shimada, H.; Imamura, M.; Matsubayashi, N.; Kikuchi, T.; Furuya, K. *J. Electron Spectrosc. Relat. Phenom.* **1999**, *88*−*91*, 817.
(43) Chen, Z. Y.; Zhao, J. P.; Yano, T.; Ooie, T. *J. Appl. Phys.* **2002**, *92*, 281.
(44) Suzuki, S.; Watanabe, Y.; Kiyokura, T.; Nath, K. G.; Ogino, T.; Heun, S.; Zhu, W.; Bower, C.; Zhou, O. *Phys. Rev. B* **2001**, *63*, 245418.
(45) Suzuki, S.; Watanabe, Y.; Ogino, T.; Heun, S.; Gregoratti, L.; Barinov, A.; Kaulich, B.; Kiskinova, M.; Zhu, W.; Bower, C.; Zhou, O. *Phys. Rev. B* **2002**, *66*, 35415.
(46) Lee, Y. T.; Kim, N. S.; Park, J.; Han, J. B.; Choi, Y. S.; Ryu, H.; Lee, H. J. *Chem. Phys. Lett.* **2003**, *372*, 853.
(47) Schroeder, S. L. M.; Moggridge, G. D.; Ormerod, R. M.; Rayment, T.; Lambert, R. M. *Surf. Sci.* **1995**, *324*, L371.
(48) Choi, H. C.; Lee, M. K.; Shin, H. J.; Kim, S. B. *J. Electron Spectrosc. Relat. Phenom.* **2003**, *130*, 85.
(49) Owens, T. M.; Süzer, S.; Banaszak Holl, M. M. *J. Phys. Chem. B* **2003**, *107*, 3177.
(50) Nishizaki, K.; Nohira, H.; Takahashi, K.; Kamakura, N.; Takata, Y.; Shin, S.; Kobayashi, K.; Tamura, N.; Hikazutani, K.; Hattori, T. *Appl. Surf. Sci.* **2003**, *216*, 287.
(51) Terrones, M.; Terrones, H.; Grobert, N.; Hsu, W. K.; Zhu, Y. Q.; Hare, J. P.; Kroto, H. W.; Walton, D. R. M.; Kohler-Redlich, Ph.; Rühle, M.; Zhang, J. P.; Cheetham, A. K. *Appl. Phys. Lett.* **1999**, *75*, 3932.
(52) Katayama, T.; Araki, H.; Yoshino, K. *J. Appl. Phys.* **2002**, *91*, 6675.
(53) Wang, X.; Hu, W.; Liu, Y.; Long, C.; Xu, Y.; Zhou, S.; Zhu, D.; Dai, L. *Carbon* **2001**, *39*, 1533.
(54) Massalski, T. B. *Binary Alloy Phase Diagrams*; American Society for Metals: Ohio, 1986.